INSTITUT FÜR ANGEWANDTE UND
NUMERISCHE MATHEMATIK

TECHNISCHE UNIVERSITÄT WIEN

Report Nr. 94/92

On the Efficient Numerical Integration of Conservation Laws with Stiff Source Terms

W. Auzinger
R. Frank
E. Weinmüller

On the Efficient Numerical Integration of Conservation Laws with Stiff Source Terms

W. Auzinger, R. Frank and E. Weinmüller

Institut für Angewandte und Numerische Mathematik
Technische Universität Wien
Wiedner Hauptstrasse 8–10/115
A-1040 Wien, Austria

1 Introduction

In our current research activity we are concerned with the numerical solution of conservation laws with stiff source terms, i.e.,

$$u_t + f(u)_x = \psi(u), \tag{1.1}$$

where the solution $u = u(x,t)$ depends on time t and some spatial variable x, and $f(u)$ is a flux function (nonlinear in general). 'Stiffness' of the source term $\psi(u)$ means that the ODE

$$\frac{du}{dt} = \psi(u) \tag{1.2}$$

is stiff, i.e., it admits solutions varying on a very fast time scale and quickly approaching smooth, that means, slowly varying solutions.

An important field of applications where conservation laws with stiff source terms arise is the study of chemically reacting gas dynamics in combustion processes. Typically, the conservation law $u_t + f(u)_x = 0$ describes the fluid dynamics of the flow considered (Euler equations). The occurrence of a stiff source term is a consequence of the modelling of rapid reactions between different chemical species.

For conservation laws without source terms a variety of reliable numerical methods is known. However, the presence of a stiff source term typically causes severe additional difficulties: The application of 'splitting' schemes, for instance (where, in each integration step, the conservation law without source term and the ODE (1.2) are solved alternatingly), will usually produce numerical artefacts with a qualitatively wrong behavior, unless extremely fine meshes are used (cf. for instance [3]). This observation motivates the search for efficient numerical methods which are able to accurately integrate the problem on a mesh which is in a natural way adapted to the variation of the solution and which is unaffected by the stiffness. In its full generality (systems of conservation laws in several space dimensions) this is a very difficult problem.

In the present report we restrict our considerations to a scalar test problem and investigate the behavior of various integration schemes. Although the scalar model considered has a relatively simple structure, it turns out that several standard approaches fail. We propose an alternative method which successfully and efficiently solves the model problem. Thus, the results presented here provide much useful information about the question which types of algorithms may be considered as possible candidates for the treatment of more general problems. However, this is of course only a first step in the development of practical algorithms; it remains to be studied whether and in what way our ideas can be successfully extended to relevant classes of conservation laws with stiff source terms.

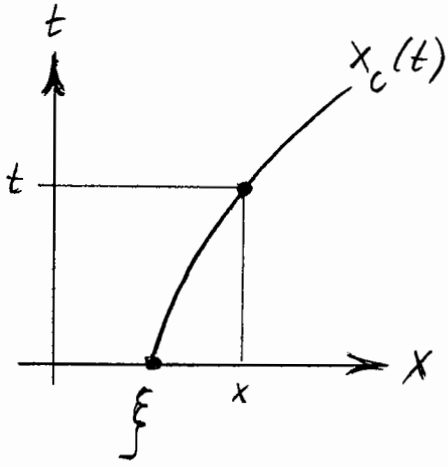

Figure 1

2 Numerical methods for scalar, spatially 1D problems

We consider the Cauchy problem for a scalar, spatially one-dimensional equation (1.1), i.e.,

$$u_t + f(u)_x = \psi(u), \qquad u(x,0) = u_0(x) \quad (x \in \mathbb{R}) \tag{2.1}$$

with given scalar data functions f, ψ and u_0, where $u_0(x) \equiv$ *const.* outside of some compact interval S.

Exact solution structure.

Let us first discuss the structure of exact solutions to a problem of the form (2.1).

Smooth solutions of this problem can by described using characteristics in the following way:

- For each ξ on the x-axis, we consider the solution of the evolution equation (cf. (1.2))

$$\frac{dv}{dt} = \psi(v), \qquad v(0) = u_0(\xi), \qquad (t \geq 0), \tag{2.2}$$

  and denote it by $v(t;\xi)$.[1]

- For each ξ, the function $v(t;\xi)$ defines an initial value problem

$$\frac{dx_c}{dt} = f'(v(t;\xi)), \qquad x_c(0) = \xi, \qquad (t \geq 0), \tag{2.3}$$

  which is simply a quadrature. The solutions $x_c(t;\xi)$ of (2.3) are curves in the (x,t)-plane starting from $x = \xi$ for $t = 0$. These curves are called the characteristics of the given problem.

- The value of a smooth solution $u(x,t)$ at some point (x,t) can now be obtained in the following way: Consider that value $\xi = \xi(x)$ for which the characteristic $x_c(t;\xi)$ passes through x at time t; then

$$u(x,t) = v(t;\xi). \tag{2.4}$$

[1] Here, the notation ξ is used for the independent variable of the initial function u_0, to avoid confusion between the independent variable x of the solution $u(x,t)$ and the starting point $\xi = \xi(x)$ of the characteristic passing through x at time t (cf. Fig. 1).

Note that for $\xi \notin S$, $u_0(\xi)$ attains some constant value by assumption, and therefore $v(t;\xi)$ does not depend on ξ in these domains. The usual case is $u_0(\xi) \equiv 0$ outside of S and $\psi(0) = 0$, implying $v(t;\xi) \equiv 0$ for $\xi \notin S$.

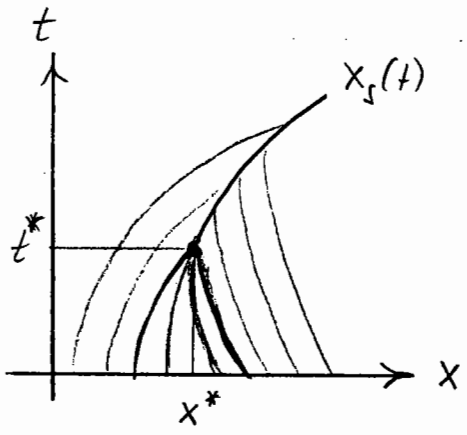

Figure 2a

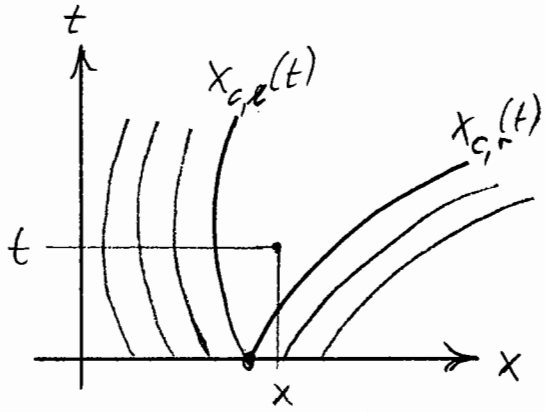

Figure 2b

If the initial function $u_0(x)$ is smooth, the solution $u(x,t)$ remains smooth as long as characteristics do not intersect. For general nonlinear problems, however, characteristics can intersect; in such cases weak solutions involving shock discontinuities appear. The case where certain points (x,t) are not reached by any characteristic corresponds the occurrence of another type of weak solutions called rarefaction waves.

Nonsmooth solutions can be described as follows[2] (cf. e.g. [5]):

- The intersection of characteristics can either occur due to a discontinuity already present in the initial profile $u_0(x)$ which is of such a nature that the characteristic directions $f'(u_\ell)$ and $f'(u_r)$ satisfy $f'(u_\ell) > f'(u_r)$ (here u_ℓ and u_r denote the left and right-hand values of $u_0(x)$ at the jump discontinuity). The other possibility is that, due to the inherent nonlinearity, characteristics originating from a smooth initial profile intersect for some $t^* > 0$, such that for $t \geq t^*$ the solution has a shock discontinuity (cf. Figure 2a).

  Let (x^*, t^*) $(t^* \geq 0)$ denote a point where such a discontinuity emerges. The 'shock line' $x_s(t)$ (i.e., that curve in the (x,t)-plane along which $u(x,t)$ has a jump) can be described by the following ODE:

$$\frac{dx_s}{dt} = \frac{f(u_\ell(x_s(t),t)) - f(u_r(x_s(t),t))}{u_\ell(x_s(t),t) - u_r(x_s(t),t)}, \qquad x_s(t^*) = x^* \qquad (t \geq t^*). \tag{2.5}$$

  Here, $u_\ell(x_s(t),t)$ and $u_r(x_s(t),t)$ denote the solution values left and right of the jump, given by $v(t;\xi_\ell)$ and $v(t;\xi_r)$, respectively, where ξ_ℓ and ξ_r are the respective starting values of the characteristics meeting at $(x_s(t),t)$.

  Equation (2.5) immediately follows from the so-called Rankine-Hugoniot jump condition, which can be derived from the weak (integral) form of the given conservation law. The Rankine-Hugoniot condition originally refers to the case $\psi \equiv 0$ (cf. e.g. [2],[5]); however, it can easily be shown that the same relation connecting the values left and right of a jump must hold in the case $\psi \neq 0$ (provided $\psi(u)$ is a smooth function). Note, however, that - despite the independence of the Rankine-Hugoniot condition of ψ - the shock curve $x_s(t)$ does depend on ψ via the values $u_\ell(x_s(t),t)$ and $u_r(x_s(t),t)$.

[2] Nonsmooth ('weak') solutions are, in general not unique. However, there usually exists a unique 'physically relevant', entropy-consistent solution, described here.

- A rarefaction wave typically occurs (cf. Figure 2b) if there is a jump discontinuity at some point ξ in the initial profile such that $f'(u_\ell) < f'(u_r)$. In this case, two characteristics $x_{c,\ell}(t)$, $x_{c,r}(t)$ emerge from ξ, and in the region $\{(x,t): \quad x_{c,\ell}(t) < x < x_{c,r}(t)\}$ a solution in the spirit of (2.2)–(2.4) is not defined. For this situation a weak solution called rarefaction wave can be constructed by applying a procedure analogous to (2.2)–(2.4), replacing the initial condition in (2.2) by a continuum of initial values, i.e.,

$$v(0) = u_\ell + \sigma(u_r - u_\ell), \qquad \sigma \in [0,1]. \tag{2.6}$$

  This completes the solution in the region $\{(x,t): \quad x_{c,\ell}(t) < x < x_{c,r}(t)\}$.

A numerical scheme imitating the true solution structure.

It is a well-known fact that conventional approaches (e.g., 'splitting' schemes where the homogeneous conservation law and the ODE (1.2) are solved alternatingly by appropriate standard methods) fail to describe the true solution behavior (concerning important quantities like shock speeds) in the presence of stiff source terms, unless extremely fine grids are used. To overcome this difficulty we have developped a scheme which directly tries to reflect the solution structure described above.

Basically, our algorithm is similar to Godunov's method, where the numerical approximations at the different time levels are piecewise constant functions. Such a piecewise constant profile defines a collection of local Riemann problems which we call a 'Multi-Riemann problem'. The original idea of Gudonov's method is to solve this Multi-Riemann problem and to approximate its solution at the next time level again by a piecewise constant function defined by averaging the Multi-Riemann solution on a fixed (usually equidistant) x-mesh. It is well known that already for problems without source terms this averaging procedure causes shocks to be 'smeared out'. Even worse, in the presence of stiff source terms such a procedure leads to dramatically incorrect shock speeds. So it seems natural to suppress the averaging process and to work with 'moving grids' instead.

This can be turned into an *algorithm* in the following way:

(i) Discretization of the initial profile $u_0(x)$ as usual (not necessarily on an equidistant x-mesh), yielding a piecewise constant initial profile.

  Choose a time step k and initialize $t_{old} := 0, \quad t_{new} := k$.

(ii) Integration of the corresponding Multi-Riemann problem for $u_t + f(u)_x = \psi(u)$ from $t = t_{old}$ up to $t = t_{new}$ by means of a numerical procedure imitating the true solution structure:

  (α) Integration of the initial value problems for $\frac{dv}{dt} = \psi(v)$, with all the constant states in the actual solution profile at $t = t_{old}$ as initial values. This can be done numerically, e.g. using the backward Euler scheme.

  This yields a set of values representing the states of the piecewise constant solution of the actual Multi-Riemann problem at $t = t_{new}$.

  (β) At grid points where $f'(u_\ell) > f'(u_r)$ we compute the corresponding local shock lines according to (2.5) above. (Note that in the case of a Riemann problem, where the states left and right of the shock line are independent of x for each fixed t, (2.5) simply reduces to a quadrature problem as soon as these states are known.) This can be done numerically, e.g. using a trapezoidal step based on the approximations for the solution left and right of the shock which are already available due to (α) above.

(γ) At grid points where $f'(u_\ell) \leq f'(u_r)$ local rarefaction waves appear. Nevertheless we treat this case in a similar way as (β) above, i.e., we compute the corresponding 'entropy-violating' local shock line according to (2.5). In the present discretization context, where any solution profile is represented by a piecewise constant function, such a procedure is reasonable provided the shape of rarefaction waves is satisfactorily reflected.

Therefore, at this point in our algorithm the cases (β) and (γ) are actually treated in a uniform way, without checking the monotonicity behavior of f'.

(δ) According to (α)–(γ), a new solution profile is defined at $t = t_{new}$. However, some additional algorithmic measures are necessary: First of all, if the distance between two neighboring jumps has become too large compared with the 'basic' stepsize used in the discretization of $u_0(x)$, new grid points are inserted using an appropriate interpolation procedure. If, on the other hand, the distance between two neighboring jumps becomes very small or if even a shock interaction occurs, grid points are deleted. In the case of a shock interaction, a new local shock line is computed emerging from the interaction point again on the basis of relation (2.5).

(iii) The process described in (ii) yields an approximation for all the local shock positions at $t = t_{new}$, and the numerical approximation is again a piecewise constant profile represented by these shock positions and the computed states in between. This procedure is now continued recursively at the following time interval, i.e., we continue with (ii) where $t_{old} := t_{new}, \quad t_{new} := t_{new} + k$.

Note that, in contrast to conventional schemes like Godunov's method, no averaging w.r.t. a fixed equidistant grid is performed. Thus our method may in short be characterized as 'shock capturing on a moving grid'. In section 3 below we will refer to this as *Method 1*.

Other methods.

In section 3 below we present a number of numerical experiments for a test problem of the type (2.1). In particular, Method 1 described above will be compared with some other numerical schemes, namely:

Method 2: Extending the Lax-Friedrichs difference formula by an evaluation of the source term $\psi(u)$ leads to the scheme[3]

$$\frac{1}{k}\Big(U_j^{n+1} - \frac{1}{2}(U_{j-1}^n + U_{j+1}^n)\Big) + \frac{1}{2h}\Big(f(U_{j+1}^n) - f(U_{j-1}^n)\Big) = \psi(U_j^{n+1}). \tag{2.7}$$

Method 3: Extending Godunov's method (which can be formally written as a conservative difference scheme) in an analogous way leads to the scheme

$$\frac{1}{k}\Big(U_j^{n+1} - U_j^n\Big) + \frac{1}{h}\Big(F(U_j^n, U_{j+1}^n) - F(U_{j-1}^n, U_j^n)\Big) = \psi(U_j^{n+1}), \tag{2.8}$$

where F denotes the corresponding numerical flux function (cf. e.g. [2], section 13 for the precise form of F).

In Methods 2 and 3, the source term is evaluated in an implicit way, i.e., at the unknown U_j^{n+1}. This is an analogue of the backward Euler discretization of the stiff ODE (1.2) and is expected to be necessary due to stability reasons. Note that this implicitness is a local one, i.e., the computation of each U_j^{n+1} requires the solution of a scalar nonlinear equation only.

[3] Here the notation U_j^n has been introduced for the numerical approximation of $u(x_j, t_n)$ where $x_j = jh$, $t_n = nk$.

Method 4: Similar to Method 1, based on the solution of a sequence of Multi-Riemann problems. However, as in the conventional Godunov scheme, the solution profiles of the Multi-Riemann problems are subject to an averaging process with respect to a fixed *equidistant* mesh $\{x_j = jh\}$, yielding the initial profile for the following Multi-Riemann problem.

Note that, in contrast to Method 1 which uses a moving grid, Methods 2–4 work on fixed, equidistant grids.

3 Numerical experiments

To investigate the robustness of the various methods w.r.t. the special difficulties caused by the presence of a stiff source term (cf. the introductory discussion in section 1), we have performed a number of numerical experiments for the following model problem proposed in [3]:

$$u_t + (u^2)_x = -\frac{1}{\tau}u(u-\tfrac{1}{2})(u-1), \qquad u(x,0) = u_0(x), \tag{3.1}$$

where $0 < \tau \ll 1$ is a small parameter characterizing the stiffness. (3.1) is Burgers' equation with a stiff source term $\psi(u)$ where the evolution equation $v' = \psi(v)$ has three stationary solutions $v \equiv 0$ (attractive), $v \equiv \frac{1}{2}$ (repelling) and $v \equiv 1$ (attractive).

In the following we present and discuss a selection of significant numerical results featuring the typical phenomena. The respective figures can be found in the Appendix. In all these figures the numerical approximations are indicated by circles, and the true solution is shown as a continuous profile.

Figures 3a and 3b demonstrate the fact that a 'naive' method like Method 2 cannot reproduce the true solution behavior: With increasing stiffness (cf. in particular Figure 3b), a completely incorrect shock speed is produced as a numerical artefact.

For Method 3, which is also simply a 'naive' extension of the conventional Godunov scheme to problems with source terms $\psi(u) \neq 0$, a similar effect occurs as can be seen from Figure 4a. For Method 4, which is based on a more sophisticated extension of the Godunov scheme, Figures 4b and 4c seem to demonstrate a remarkable robustness with respect to increasing stiffness: The shock speed is reflected correctly on the coarse grid used. Note, however, that the initial profile in Figures 3 a,b and 4 a,b,c is very special because the Riemann data are chosen exactly as the stable stationary values of the ODE $v' = \psi(v)$ such that no rapid variation (transient phase) occurs; the solution is constant left and right to the shock.

In Figure 5, the Riemann data have been chosen such that the true solution $u(x,t)$ varies rapidly in t: The initial values left and right to the discontinuity are such that the fast time scale is activated (there occur transient solutions of the stiff ODE $v' = \psi(v)$). In such a situation, also Method 4 produces an incorrect shock speed. An extremely small time step k would be necessary in the transient phase to overcome this problem.

Figures 6 a,b,c show that our Method 1 successfully resolves the true solution behavior on coarse grids. Problems with increasing stiffness and the occurrence of a transient phase are correctly handled, in particular concerning shock speeds. The numerical errors appearing for small t are due to the relatively large time step used and due to the fact that in Method 1 the ODE $v' = \psi(v)$ is solved simply by an implicit Euler step. However, for larger values of t the numerical solution correctly converges, including a precise reproduction of the shock speed (cf. Figures 6 b,c).

A more general initial profile has been used for Figures 7 a,b,c. Also in this situation, Method 1 performs satisfactorily.

In Figures 8 a,b,c the initial data would produce a shock-free solution in the case $\psi(u) = 0$. The influence of a stiff source term $\psi(u) \neq 0$, however, forces the solution profile to be very steep. Also this difficulty is coped with successfully by Method 1.

Finally, Figures 9 a,b,c show the results for the same data as in Figures 8 a,b,c but with Method 3 instead of Method 1. The propagation of the the steep solution profile is not correctly reproduced.

4 Conclusions

The numerical results presented in section 3 have been selected from a long series of experiments. All these results show that only 'Method 1' is able to successfully integrate the model problem (3.1):

- Shock speeds are correctly reproduced, also for very stiff problems (τ very small), using grids that can be chosen independent of τ and that are only adjusted to the smoothness of the solutions away from the shock.

- Also in the presence of a transient phase for small t, large time steps can be used throughout. In this case the transient phase itself is not precisely resolved but it can be observed that after the transient phase the solution is again accurately tracked.

Thus the approach behind Method 1 is superior, in these respects, to many others appearing in the literature (cf. for instance [1], [3] where the occurrence of incorrect shock propagation speeds is also observed for a variety of conventional schemes, including 'splitting' approaches). However, recently also other schemes have been proposed for the handling of stiff source terms (e.g. shock tracking approaches like the one described in [4]). To our opinion, a major advantage of Method 1 is the automatic, precise capturing of shock discontinuities, where – similarly as in Godunov's method for problems without source terms – no decision is necessary whether a jump between two neighboring discrete states is 'infinitesimal' (that is, a discretization of a smooth profile) or a true discontinuity (that is, a discretization of a shock).

The crucial question is whether it is possible to successfully apply these ideas to more realistic hyperbolic conservation laws with stiff source terms. Thus our current research activities concentrate on the following questions:

- Other schemes proposed in the literature (cf. e.g. [4]) will be directly compared to Method 1 for the model equation (3.1); in particular, the robustness with respect to the stiffness and the occurrence of rapidly transient solutions will be systematically investigated.

- Method 1 or other promising methods will be appropriately extended to spatially one-dimensional systems of conservation laws with stiff source terms. One main goal is the efficient integration of the Euler equations of gas dynamics in one space dimension with one (or several) additional equation(s) describing a chemical reaction:

$$(\rho)_t + (\rho v)_x = 0 \tag{4.1a}$$
$$(\rho v)_t + (\rho v^2 + p)_x = 0 \tag{4.1b}$$
$$(E)_t + ((E+p)v)_x = 0 \tag{4.1c}$$
$$(\rho Z)_t + (\rho v Z)_x = -K(T)\rho Z \tag{4.1d}$$

Here, ρ, v, E, and p denote the densitiy, velocity, energy and pressure, respectively. $T = \frac{p}{\rho R}$ (R ... gas constant) is the absolute temperature; Z denotes the unburnt gas fraction. Equation

(4.1d) models the chemical reaction; in a combustion process this reaction takes place on a very fast time scale, such that the source term $-K(T)\rho Z$ is typically stiff. A standard ansatz for the function $K(T)$ would be given by the Arrhenius model

$$K(T) = K_0 T^{\alpha} e^{-A/T} \tag{4.2}$$

with certain constants K_0, α and A.

The essential difficulty with (4.1) is given by the fact that the Euler equations (4.1a–4.1c) and the scalar equation (4.1d) (with stiff source term) are fully coupled: Note, in particular, that the energy E depends also on Z due to the relation

$$E = \frac{p}{\gamma - 1} + \frac{1}{2}\rho v^2 + q_0 \rho Z \tag{4.3}$$

with certain constants γ and q_0.

It is well known that the usual splitting approach – where the system (4.1) *without* source term and the ODE $u' = -K(T)u$ (with an appropriately 'frozen' $K(T)$) are solved alternatingly – is not robust with respect to increasing stiffness. Therefore our goal is to apply a more direct approach. One simple idea would be to consider, at each time step, each of the scalar equations (4.1a–4.1d) separately and to solve it for the respective unknown, where the values of the other unknowns are 'frozen' for the moment, i.e., their values available from the preceding time level are used as data functions for the scalar equation considered. In each step of such a procedure, Method 1 (designed for scalar equations) could be applied. This would mean that each unknown has an individual, moving grid associated with it. (The necessary transfer of values between these grids has to be performed by means of appropriate averaging processes.) Such a procedure can, if necessary, also be iterated within a fixed time step in a predictor-corrector sense.

It is, however, not clear at the moment whether such or a similar procedure will lead to a satisfactory numerical method for problems of the type (4.1), and how varios open details should be implemented. This idea may also still be too naive, such that more complex and powerful extensions of Method 1 to the vector case would be necessary imitating more closely the true solution structure.

- The treatment of systems of conservation laws with source terms in several space dimensions is, of course, the ultimate goal of all these activities. Whether the above ideas can be successfully generalized to this most general situation is still uncertain.

References

[1] P. Colella, A. Majda, V. Roytburd, *Theoretical and Numerical Structure for Reacting Shock Waves*, SIAM Journal of Scientific and Statistical Computing 7, 1059–1080 (1986).

[2] R. J. Leveque, *Numerical Methods for Conservation Laws*, Birkhäuser, 1990.

[3] R. J. Leveque, H. C. Yee, *A Study of Numerical Methods for Hyperbolic Conservation Laws with Stiff Source Terms*, Journal of Computational Physics 86, 187–210, (1990).

[4] R. J. Leveque, K. M. Shyue, *Shock Tracking Based on High Resolution Wave Propagation Methods*, Research Report No. 92-01, Seminar für Angewandte Mathematik, ETH Zürich, 1992.

[5] J. Smoller, *Shock Waves and Reaction-Diffusion Equations*, Springer, 1983.

Appendix

Figure 3a:

- Initial profile:

$$u_0(x) = \begin{cases} 1, & x \leq 0, \\ 0, & x > 0 \end{cases}$$

- $\tau = 0.01$
- Method 2
- $h = 0.1, \quad k = 0.1$
- Result shown for $t = 1.0$

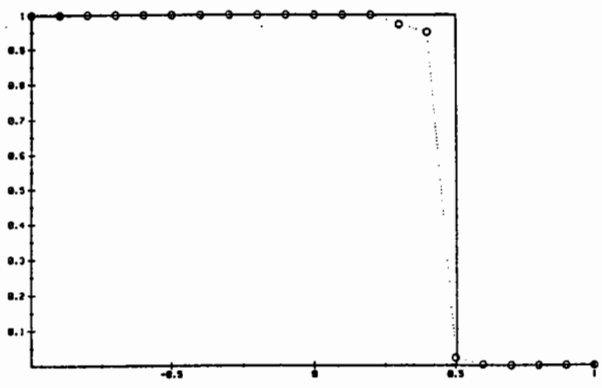

Figure 3b:

- Initial profile:

$$u_0(x) = \begin{cases} 1, & x \leq 0, \\ 0, & x > 0 \end{cases}$$

- $\tau = 0.001$
- Method 2
- $h = 0.1, \quad k = 0.1$
- Result shown for $t = 1.0$

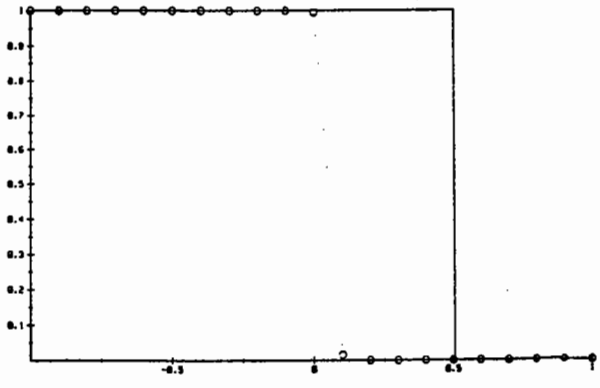

Figure 4a:

- Initial profile:

$$u_0(x) = \begin{cases} 1, & x \leq 0, \\ 0, & x > 0 \end{cases}$$

- $\tau = 0.001$
- Method 3
- $h = 0.1, \quad k = 0.1$
- Result shown for $t = 1.0$

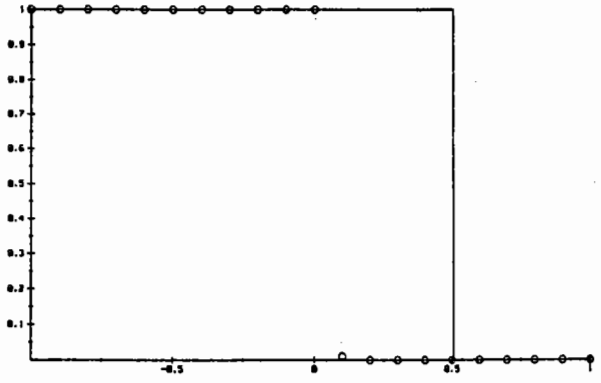

Figure 4b:

- Initial profile:

$$u_0(x) = \begin{cases} 1, & x \leq 0, \\ 0, & x > 0 \end{cases}$$

- $\tau = 0.001$
- Method 4
- $h = 0.1, \quad k = 0.1$
- Result shown for $t = 1.0$

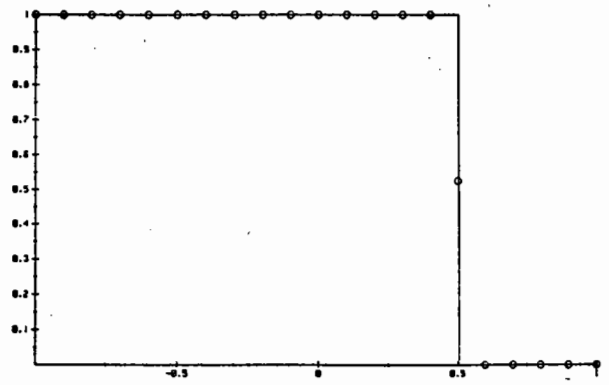

Figure 4c:

- Initial profile:

$$u_0(x) = \begin{cases} 1, & x \leq 0, \\ 0, & x > 0 \end{cases}$$

- $\tau = 0.0001$
- Method 4
- $h = 0.1, \quad k = 0.1$
- Result shown for $t = 1.0$

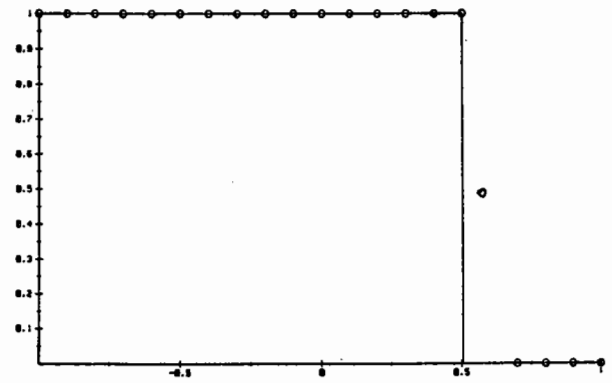

Figure 5:

- Initial profile:

$$u_0(x) = \begin{cases} 2, & x \leq 0, \\ -1, & x > 0 \end{cases}$$

- $\tau = 0.001$
- Method 4
- $h = 0.1, \quad k = 0.05$
- Result shown for $t = 1.0$

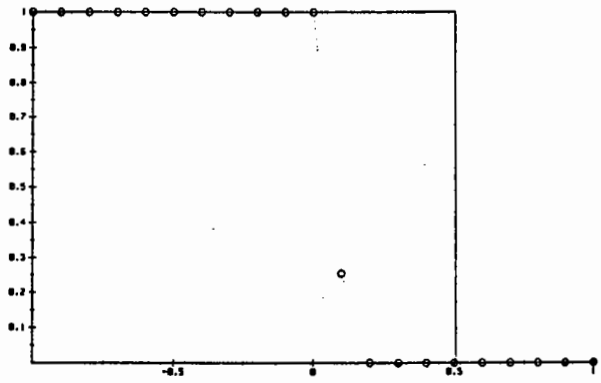

Figure 6a:

- Initial profile:

$$u_0(x) = \begin{cases} 1, & x \leq 0, \\ 0, & x > 0 \end{cases}$$

- $\tau = 0.0001$
- Method 1
- $h = 0.1, \quad k = 0.1$
- Result shown for $t = 1.0$

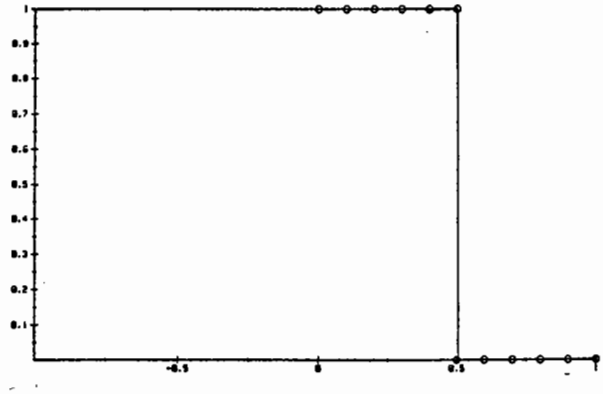

Figure 6b:

- Initial profile:

$$u_0(x) = \begin{cases} 2, & x \leq 0, \\ -1, & x > 0 \end{cases}$$

- $\tau = 0.001$
- Method 1
- $h = 0.1, \quad k = 0.05$
- Result shown for $t = 0.05$

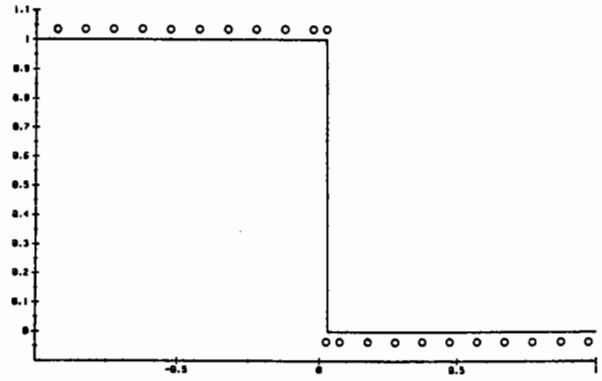

Figure 6c:

- Initial profile:

$$u_0(x) = \begin{cases} 2, & x \leq 0, \\ -1, & x > 0 \end{cases}$$

- $\tau = 0.001$
- Method 1
- $h = 0.1, \quad k = 0.05$
- Result shown for $t = 1.0$

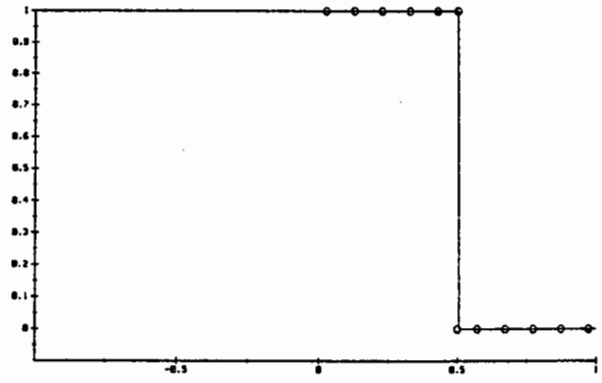

Figure 7a:

- Initial profile:

$$u_0(x) = \begin{cases} 1, & x \leq \frac{\pi}{2}, \\ -\sin x, & -\frac{\pi}{2} \leq x < \frac{\pi}{2}, \\ -1, & x \geq \frac{\pi}{2} \end{cases}$$

- $\tau = 0.01$
- Method 1
- $h = 0.1, \quad k = 0.1$
- Result shown for $t = 0.1$

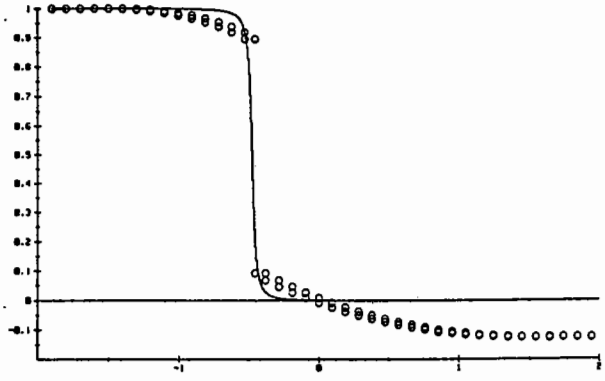

Figure 7b:

- Initial profile:

$$u_0(x) = \begin{cases} 1, & x \leq \frac{\pi}{2}, \\ -\sin x, & -\frac{\pi}{2} \leq x < \frac{\pi}{2}, \\ -1, & x \geq \frac{\pi}{2} \end{cases}$$

- $\tau = 0.01$
- Method 1
- $h = 0.1, \quad k = 0.1$
- Result shown for $t = 0.2$

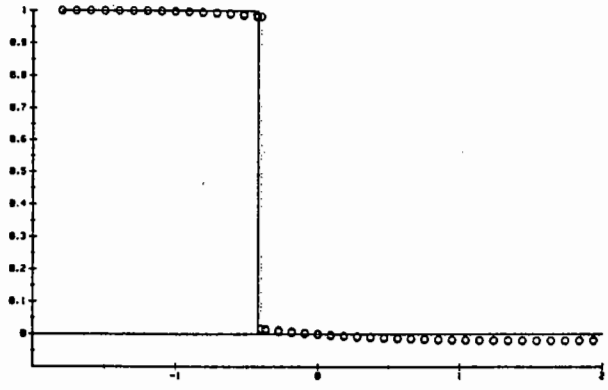

Figure 7c:

- Initial profile:

$$u_0(x) = \begin{cases} 1, & x \leq \frac{\pi}{2}, \\ -\sin x, & -\frac{\pi}{2} \leq x < \frac{\pi}{2}, \\ -1, & x \geq \frac{\pi}{2} \end{cases}$$

- $\tau = 0.01$
- Method 1
- $h = 0.1, \quad k = 0.1$
- Result shown for $t = 1.0$

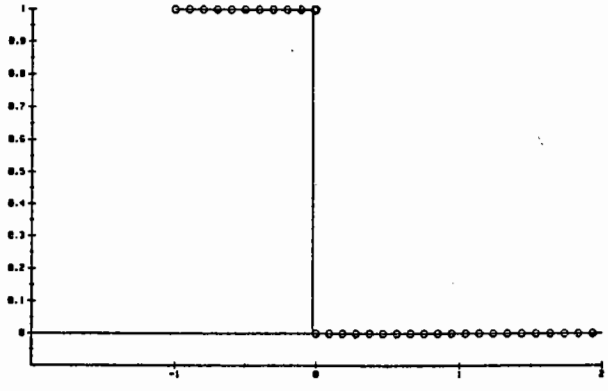

Figure 8a:

- Initial profile:

$$u_0(x) = \begin{cases} -1, & x \le -1, \\ x, & -1 \le x < 1, \\ 1, & x \ge 1 \end{cases}$$

- $\tau = 0.01$
- Method 1
- $h = 0.01, \quad k = 0.01$
- Result shown for $t = 0.1$

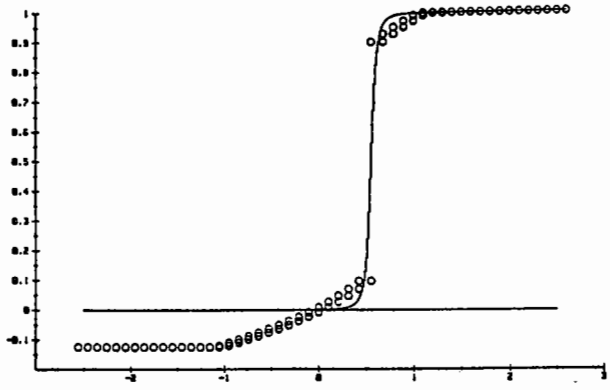

Figure 8b:

- Initial profile:

$$u_0(x) = \begin{cases} -1, & x \le -1, \\ x, & -1 \le x < 1, \\ 1, & x \ge 1 \end{cases}$$

- $\tau = 0.01$
- Method 1
- $h = 0.01, \quad k = 0.01$
- Result shown for $t = 0.2$

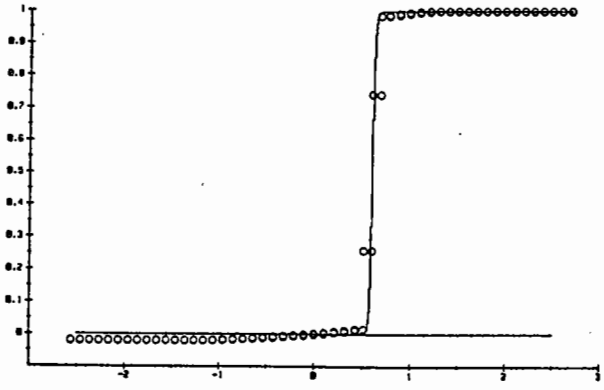

Figure 8c:

- Initial profile:

$$u_0(x) = \begin{cases} -1, & x \le -1, \\ x, & -1 \le x < 1, \\ 1, & x \ge 1 \end{cases}$$

- $\tau = 0.01$
- Method 1
- $h = 0.01, \quad k = 0.01$
- Result shown for $t = 1.0$

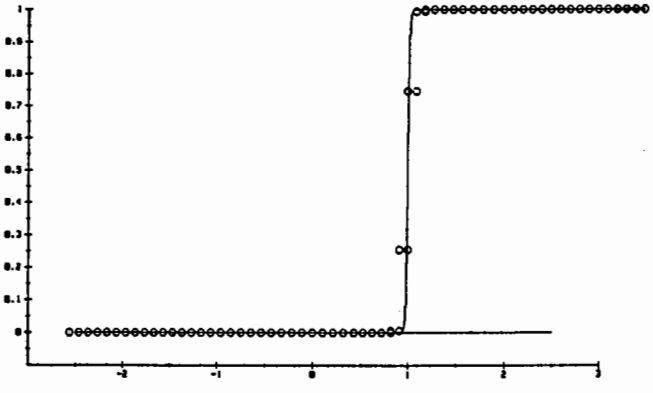

Figure 9a:

- Initial profile:

$$u_0(x) = \begin{cases} -1, & x \le -1, \\ x, & -1 \le x < 1, \\ 1, & x \ge 1 \end{cases}$$

- $\tau = 0.01$
- Method 3
- $h = 0.01, \quad k = 0.01$
- Result shown for $t = 0.1$

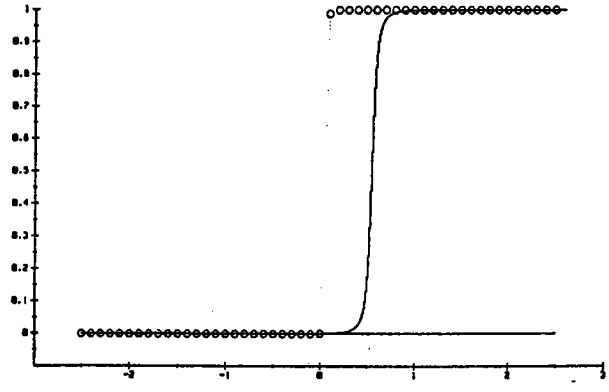

Figure 9b:

- Initial profile:

$$u_0(x) = \begin{cases} -1, & x \le -1, \\ x, & -1 \le x < 1, \\ 1, & x \ge 1 \end{cases}$$

- $\tau = 0.01$
- Method 3
- $h = 0.01, \quad k = 0.01$
- Result shown for $t = 0.2$

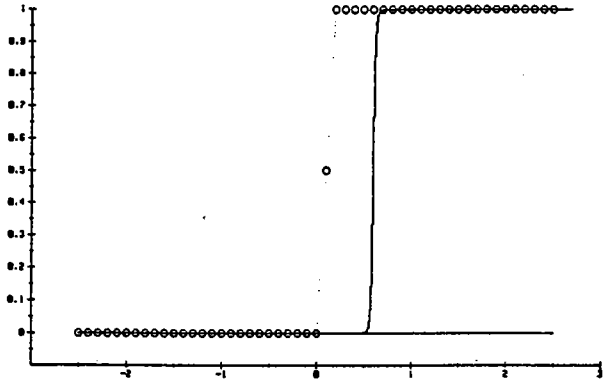

Figure 9c:

- Initial profile:

$$u_0(x) = \begin{cases} -1, & x \le -1, \\ x, & -1 \le x < 1, \\ 1, & x \ge 1 \end{cases}$$

- $\tau = 0.01$
- Method 3
- $h = 0.01, \quad k = 0.01$
- Result shown for $t = 1.0$